On the Inner Structure and Topology of Clusters in Two-Component Lipid Bilayers. Comparison of Monomer and Dimer Ising Models

ARTICLE *in* THE JOURNAL OF PHYSICAL CHEMISTRY B · SEPTEMBER 2008

Impact Factor: 3.3 · DOI: 10.1021/jp800945j · Source: PubMed

1 AUTHOR:

Istvan Sugar
Icahn School of Medicine at Mount Sinai
80 PUBLICATIONS **1,416** CITATIONS

SEE PROFILE

On the Inner Structure and Topology of Clusters in Two-Component Lipid Bilayers. Comparison of Monomer and Dimer Ising Models

István P. Sugár

Department of Neurology, Mount Sinai School of Medicine, New York, New York 10029

Received: January 31, 2008; Revised Manuscript Received: June 20, 2008

It has been shown on model and biological systems that membrane clusters can affect in-plane membrane reactions and can control biochemical reaction cascades. Clusters of two-component phospholipid bilayers have been simulated by two Ising-type lattice models: the monomer and the dimer model. In each model the plane of one layer of the bilayer is represented by a triangular lattice, each site of which is occupied by an acyl chain of either a component 1 or a component 2 lipid molecule. The dimer model assumes that pairs of acyl chains (lipid molecules) are permanently connected, forming dimers on the lattice, while in the case of the monomer model this covalent connection between acyl chains is ignored. Phase diagrams of two-component phospholipid bilayers were successfully calculated by both models. In this work, we use Monte Carlo techniques to calculate thermodynamic averages of global and local characteristics of the largest component 2 cluster (such as outer/inner perimeter, percolation, minimal linear size, and local density) and compare the results obtained by the two models. A new method is developed to characterize the inner structure of the clusters. Each point of a cluster is classified based on its shortest distance (or depth) from the cluster's outer perimeter. Then local cluster properties, such as density, are calculated as a function of the depth. The depth analysis reveals that toward the cluster interior the average density usually decreases in midsize clusters and remains constant in very large clusters. On the basis of the simulations the following typical cluster topologies are identified at different cluster sizes and cooperativity parameter values: (i) branch-like, (ii) circular, (iii) band-like, and (iv) planar.We did not find qualitative differences between the cluster structures in the dimer and monomer model. However, at the same cluster size and cooperativity parameter value the cluster of the dimer model is more compact. The cluster properties of the dimer model are different from that of the monomer model because of the lower mixing entropy and higher formation energy of an elementary inner island.

Introduction

The idea that cluster formation in biological membranes can influence protein activity and function was first expressed in the early 70s.[1,2] It has been shown on model and biological systems that membrane clusters can control biochemical reaction cascades.[3−7] It was found that gel-to-fluid transition, i.e.: the coexistence of fluid and gel clusters, can trigger phospholipase A_2 activity.[8−10] Changes in the opening times of calcium channels, reconstituted in POPE/POPC membranes, have been interpreted as a consequence of fluid-gel coexistence in the lipid membrane.[11] It was shown that lateral heterogeneities of the lipid membrane control the activation of protein kinase C.[12,13] A connection was also found between the activity of calcium ATPase and the lipid structure of the plasma membrane.[14]

Biological membranes are composed of proteins embedded fully or partially into a lipid matrix. The majority of the hundreds of membrane lipid components have a polar headgroup with two acyl chains attached to it. In order to study the structure of the lipid matrix, such as the clustering of lipid molecules, two-component lipid bilayers—simplified model systems of the biological membranes—have been investigated both experimentally and theoretically for decades. Lipid bilayers are collective systems. Their structural and thermodynamic properties cannot be understood by investigating their units, the lipid molecules, without paying attention to the interactions between these units.

The first theoretical model of a collective system, the model of ferromagnets, was developed by Ernst Ising[17] in 1925. Ever since, similar models have been used to model a broad range of collective systems. Two-component lipid bilayers have also been modeled by two-dimensional Ising-type lattice models, where the plane of one layer of the bilayer is represented by a triangular lattice. In attempts to perform a Monte Carlo simulation of a two-component bilayer on the lattice, three options have generally been envisaged.

The first is to consider that the acyl chains occupy the lattice sites and behave independently from each other. This, the so-called *monomer model*, provides the correct lattice geometry but ignores covalent connection between the chains of a lipid molecule.[18−21] In Figure 1a, a monomer model is shown where open and closed circle represents the acyl chain of a component 1 and a component 2 molecule, respectively.

The second, the so-called *dimer model*, takes into account the fact that the majority of membrane lipids possess two covalently coupled acyl chains. It is assumed that the acyl chains of the lipids occupy the sites of a triangular lattice and that pairs of chains (lipid molecules) are permanently connected, forming dimers on the lattice.[22−29] In Figure 1b, a dimer model is shown where a lipid molecule is represented by a pair of nearest neighbor circles connected by a straight line. Component 1 and component 2 molecule is a connected pair of open and pair of closed circles, respectively.

10.1021/jp800945j CCC: $40.75
Published on Web 08/26/2008

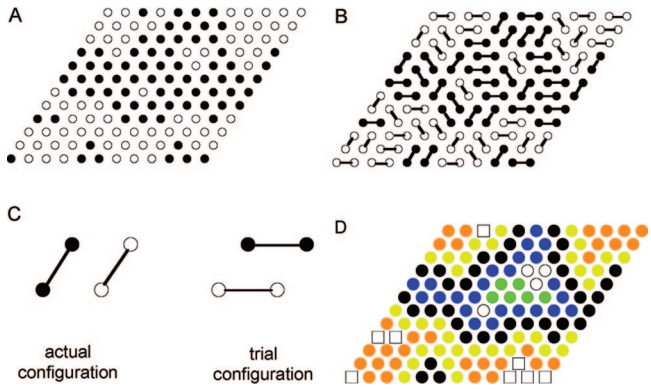

Figure 1. Illustrations of the monomer and dimer model of two-component lipid bilayers: (a) The monomer model of two-component lipid bilayer. One layer of the bilayer is represented by a triangular lattice, each site of which is occupied by an acyl chain of either component 1 (open circle) or component 2 (closed circle) lipid molecule. The model ignores the covalent connection between the acyl chains of the lipid molecules. (b) The dimer model of two-component lipid bilayer. One layer of the bilayer is represented by a triangular lattice, each site of which is occupied by an acyl chain of either component 1 (open circle) or component 2 (closed circle) lipid molecule. The dimer model assumes that pairs of acyl chains (lipid molecules) are permanently connected, forming dimers (pairs of circles connected by solid lines) on the lattice. (c) Illustration of the trial configuration generation in the case of the dimer model. In this illustration the actual and the trial configuration contain different types of molecules. However one can select a pair of similar molecules as well and generate the trial configuration. Trial configuration can be generated only if the nodes of the selected pair of molecules define a rhombus. (d) Snapshot and cluster characteristics. In the snapshot different characteristics of the largest component 1 and largest component 2 cluster are color-coded. Yellow and orange dots mark the elements of the largest component 1 cluster, while black, blue and green dots mark the 1st, 2nd and 3rd depth levels of the largest component 2 cluster, respectively. Yellow and black dots show the outer periphery of the largest component 1 and largest component 2 clusters, respectively. Open circles and open squares mark the small component 1 and component 2 clusters inside the largest component 2 and largest component 1 cluster, respectively.

The third is to consider that each lipid molecule occupies one lattice site.[30−32] This choice, however leads to an incorrect lattice geometry, because it is the acyl chains, and not the lipids as a whole, that occupy sites having a coordination number of ($z = 6$).[16]

The phase diagrams of two-component lipid bilayers were successfully calculated by both the monomer and dimer models.[18,19,23,24] In this work we investigate side by side the structure and topology of the compositional clusters of these models. By using Monte Carlo techniques, we calculate thermodynamic averages of global and local characteristics of the largest component 2 cluster and compare the results obtained by the two models.

Model

In this paper, we model one layer of symmetric lipid bilayers. In the past, we developed a similar Ising-like dimer model of two-component lipid bilayers.[23] In that model, each lipid component could exist in either gel or fluid state.

In contrast to our above-mentioned dimer model, in this paper we consider one layer of the two-component lipid bilayer in either pure gel or pure fluid phase.

Lattice Geometry and Configuration. One layer of a bilayer is modeled as a triangular lattice of n rows and n columns (coordination number $z = 6$). n_1 lattice points are occupied by the acyl chains of component 1 and $n_2(=n^2 - n_1)$ lattice points are occupied by the acyl chains of component 2 lipid molecules. In case of the *dimer model* pairs of chains (lipid molecules) are permanently connected, forming dimers on the lattice (see Figure 1b), while in the case of the *monomer model* the connection is ignored (see Figure 1a).

In the case of the monomer model the actual configuration of the lattice is defined by the component type at every lattice point. In the case of the dimer model the actual configuration of the lattice is defined by the location and orientation of each component 1 and component 2 dimer.

When calculating the energy of a configuration only nearest-neighbor interactions are considered. This is the case because the acyl chains of the lipid molecules interact through short-range van der Waals interactions. There are three interaction energies: E_{11}, E_{22}, and E_{12} between the nearest neighbor lattice points occupied by acyl chains of components 1−1, 2−2, and 1−2, respectively.

The energy of a configuration is:

$$E = E_1 n_1 + E_2 n_2 + E_{12} n_{12} + E_{11} n_{11} + E_{22} n_{22} \quad (1)$$

where n_{ij} is the number of nearest neighbor lattice points occupied by acyl chains of components $i-j$, and E_i is the intra chain energy of component i. In the case of periodic boundary condition the following two additional relationships hold:[24]

$$z n_1 = 2 n_{11} + n_{12} \quad (2)$$

$$z n_2 = 2 n_{22} + n_{12} \quad (3)$$

After substituting eqs 2 and 3 into eq 1 we get

$$E = (E_1 + z E_{11}/2) n_1 + (E_2 + z E_{22}) n_2 + n_{12}[E_{12} - (E_{11} + E_{22})/2] \quad (4)$$

By introducing periodic boundary conditions, we eliminate lattice edge effects and reduce the number of model parameters. If the mixing ratio is constant, the energy difference between configuration a and configuration b is:

$$\Delta E = w(n_{12}^b - n_{12}^a) = w \Delta n_{12} \quad (5)$$

where the only model parameter is the cooperativity parameter, w [$=E_{12} - (E_{11} + E_{22})/2$].

Monte Carlo Methods. It is assumed that the bilayer is in thermal interaction with the surrounding. By using Monte Carlo methods one can simulate the thermal fluctuations of the two-component bilayer. The thermal fluctuations are manifested in the fluctuation of the bilayer energy and in the ever changing lattice configuration.

The steps of each Monte Carlo simulation are as follows: (1) creating an initial configuration; (2) creating a trial configuration; (3) decision making (accepting or rejecting the trial configuration); (4) returning to step 2. This procedure can be viewed as a chain of trial configuration generations.

Initial Configurations and Trial Configurations. In the case of the monomer model each simulation starts from a configuration where the acyl chains of the components are randomly distributed. A trial configuration is generated from an actual configuration by exchanging two randomly selected acyl chains of different lipid components. A trial configuration is accepted if

$$\text{ran} < \mathrm{e}^{-(E_t - E_a)/kT} = e^{-(w/kT)(n_2^t - n_2^a)} \quad (6)$$

where *ran* is a random number generated between 0 and 1, k is the Boltzman constant, T is the absolute temperature, E_t and E_a are the energies of the trial and actual configurations, respec-

tively. The energy difference in eq 6 is calculated by means of eq 5. n_{12}^t and n_{12}^a are the number of nearest-neighbor chains of component 1 and 2 in the trial and actual configuration, respectively. The trial configuration is rejected if the inequality in eq 6 is not fulfilled.[33] This method of decision making drives the system toward thermodynamic equilibrium, the Boltzman distribution over the configurations, independent of the initial configuration.

In the case of the dimer model the simulation starts from a regular arrangement. Each molecule, i.e., dimer, is oriented horizontally. Component 1 molecules are assigned to the first n_1 lattice points. A trial configuration is generated as follows: two nearest neighbor lattice points are randomly selected. If these points belong to two similarly oriented molecules, where the respective acyl chains define the nodes of a rhombus, then one can generate the trial configuration by exchanging the acyl chains on the opposite nodes of the rhombus (see Figure 1c). This exchange involves a rotation of the respective molecules by $\pm 60°$. The trial configuration is accepted again according to the criterion given by eq 6. A series of these elementary reorientations leads to the equilibrium distribution of the orientation of the molecules. Note that, like the exchange of different acyl chains, the reorientation results in the lateral movement of the molecules too. Thus a series of reorientation steps is able to drive the system to the equilibrium of the lateral distribution of the molecules.

Monte Carlo Cycles. The chain of trial configuration generation can be divided into Monte Carlo cycles. During each Monte Carlo cycle the system has the *opportunity* to realize all of its configurations at least once. In the case of the monomer model each Monte Carlo cycle consists of n_1 (or n_2 if $n_2 < n_1$) trial configuration generations.

In the case of the dimer model in each Monte Carlo cycle $2n^2$ trial configuration generations are performed.

At the beginning of a Monte Carlo simulation equilibration cycles are performed until the characteristic extensive parameter(s) of the system, such as energy, starts to fluctuate around a constant value. After attaining the equilibrium distribution the snapshots are analyzed at the end of each Monte Carlo cycle, and the results are stored for further statistical analyses.

Snapshot Analysis and Lattice Statistics. The snapshot analysis takes place by means of a cluster counting algorithm[34] that labels each cluster in a snapshot with a different number. The periodic boundary conditions are taken into consideration during the labeling procedure.

Outer and Inner Periphery of the Largest Component 2 Cluster. After the cluster labeling the largest component 1 and largest component 2 clusters are selected from the snapshot. The size of a cluster is defined by the number of lattice points belonging to the cluster. The cluster points at the interface of the two largest clusters define the outer peripheries of these two clusters. By counting the component 2 cluster points at the interface we get the outer periphery of the largest component 2 cluster.

A cluster point is either peripheral or inner. Every nearest neighbor of an inner point is itself a cluster point, while in the case of a peripheral point there is at least one nearest neighbor that is not part of the cluster. By using this definition of inner and peripheral points one can count the number of inner and peripheral points in the largest component 2 cluster of the snapshot. Note that this way one counts the total number of peripheral points, i.e., points forming both the outer and inner periphery of the largest component 2 cluster. Inside the largest component 2 cluster there are small component 1 clusters, the so-called inner islands. If an inner island is located deep inside the large cluster, it is surrounded exclusively by inner peripheral points. However, if it is at the edge of the large cluster, it is surrounded by both outer and inner peripheral points. In Figure 1d a snapshot of the monomer model is shown where the different characteristics of the largest component 1 and largest component 2 cluster are color-coded.

Depth Analysis of the Largest Component 2 Cluster. So far we have classified three types of lattice points; points belonging to the (i) cluster interior, (ii) outer periphery, and (iii) inner periphery. One can also classify cluster points according to their "distance" or "depth" from the outer perimeter. The depth of the points of the outer perimeter is defined to be 1. Now let us consider the rest of the cluster points. A point's depth is 2 if it has at least one nearest neighbor that belongs to the outer periphery, i.e., to depth 1. This way one can find every cluster point of depth 2. Continuing the above procedure one can assign a depth to each remaining cluster point. The number of cluster points that belongs to depth k is marked by d_k. The deepest point (or points) can be considered as the *central point* (or points) of the cluster. The *minimal linear size* (MLS) of the cluster at the cluster's center can be defined as $\mathrm{MLS} = 2c - 1$, where c is the depth of the central point(s). With this definition MLS = 1 for a one-dimensional cluster. In Figure 1d, the largest component 2 cluster has three depth levels. Levels 1, 2, and 3 are encoded by black, blue, and green dots, respectively. Each contains $d_1 = 36$, $d_2 = 24$, and $d_3 = 6$ lattice points. According to our above definition in Figure 1d, the largest component 2 cluster has 6 central points and its MLS is 5.

Local Density in the Cluster. One can determine the local density of component 1 at the i-th point of the largest component 2 cluster as follows:

$$\rho_i = \frac{n_i}{7} \tag{7}$$

where n_i is the number of component 1 lattice points from the six nearest neighbors of the ith point of the component 2 cluster. One can determine the local density, ρ_i^k at every cluster point of depth k and calculate the average local density at depth k:

$$\langle \rho^k \rangle = \sum_{i=1}^{d_k} \rho_i^k / d_k \tag{8}$$

Percolation Frequency of the Cluster. A cluster is percolated if it spans the lattice from left to the right or bottom to the top edge.[34] We consider those snapshots of the Monte Carlo simulation where the size of the largest component 2 cluster is the same, N. Then we determine the proportion of snapshots where the largest component 2 cluster is percolated. This proportion is the so-called percolation frequency of clusters of size N.

Parameters of the Simulations. Complete simulations were performed at the following w/kT parameter values: 0, 0.15, 0.3, 0.33, 0.36, 0.39, 0.42, and 0.45. These numbers are within the range of w/kT values obtained for DMPC/DSPC two-component lipid bilayer.[23] In order to further explore the phase space of the monomer model, additional simulations were performed at higher w/kT values up to 1.4. Each simulation was performed on a 40×40 triangular lattice. This lattice size was sufficient to calculate excess heat capacity curves of DMPC/DSPC binary mixtures in agreement with the experimental data.[23,29]

In the case of the monomer model, after 5000 equilibration cycles we ran 20 000 cycles and analyzed the snapshots at the

end of each of these cycles. In the case of the dimer model first we ran 1000 cycles with $w/kT = 0.0$ in order to randomize the location and orientation of the molecules. Then we set w/kT to its respective value. After another 4000 equilibration cycles we ran 100 000 cycles and analyzed the snapshots at the end of each cycle. Finally the averages of the cluster characteristics were calculated. Separate simulations have been run at different compositions. In the above-described simulations the number of chains of component 2 was changed from 6 to 1580.

Results and Discussions

After equilibration the snapshot at the end of every Monte Carlo cycle was analyzed. During the analysis the largest component 2 cluster was selected and the following properties were determined and stored for further statistical analysis: cluster size, outer periphery, inner periphery, number of cluster points at different depths, local density of component 1 chains at each cluster point, percolatedness of the cluster, and size of the largest component 1 cluster. At the end of the simulation the average of each of these properties were calculated. The average outer (and inner) perimeter vs cluster size curves inform us about the overall compactness and topology of the clusters. The average density vs depth curves reveal the distribution of the inner islands within the largest component 2 cluster. The percolation frequency vs cluster size curves show how frequently a cluster of certain size spans the lattice from its left to the right or from its top to the bottom edge. The different average cluster properties calculated from the monomer and dimer model are plotted side by side.

Total Cluster Perimeter. In Figure 2, the average total perimeter of the cluster is plotted against the cluster size. Each curve belongs to a different value of the w/kT parameter. In the case of each model at $w/kT = 0$, the curve increases linearly and the number of peripheral points is close to the cluster size; i.e., almost every point of the cluster is peripheral. The curve, however, starts to deviate from the straight line at about 700. From this cluster size the number of nonperipheral, i.e., inner, cluster points increases at a higher rate. At about 1200 the curve reaches its maximum, i.e. the number of peripheral points start decreasing, until every point becomes an inner cluster point at 1600. At $w/kT > 0$, in the case of the monomer model, the character of the curves remain similar, but internal points appear even at small cluster sizes. At $w/kT \geq 1.1$, the total perimeter curves are almost flat from cluster size 600 to 1000. In this size range the cluster has a topologically band-like shape (see next section).

In the case of the dimer model increasing values of w/kT reduce the cluster perimeter at a much faster rate than in the monomer model. Also the band-like cluster shape appears at a much lower value of the cooperativity parameter, $w/kT \approx 0.36$.

Cluster's Outer and Inner Perimeter. In Figures 3 and 4, the average number of outer and inner peripheral points are plotted, respectively against cluster size. On the basis of the comparison of the inner peripheries, one can say that the clusters of the dimer model are more compact than the respective clusters of the monomer model. Both the outer and inner perimeter increases up to about cluster size 700; however, the increase of the outer perimeter is more than twice as fast.

At $w/kT = 0$, when the outer perimeter is maximal, about 500, the inner perimeter is about 180. Above cluster size 700 the outer perimeter sharply decreases while the inner perimeter sharply increases. The inner perimeter becomes maximal, almost 1000 for the monomer model (and 800 for the dimer model), at cluster size 1200. By this cluster size the outer perimeter drops to about 30. These sharp transition from outer to inner periphery will be discussed in the next two sections.

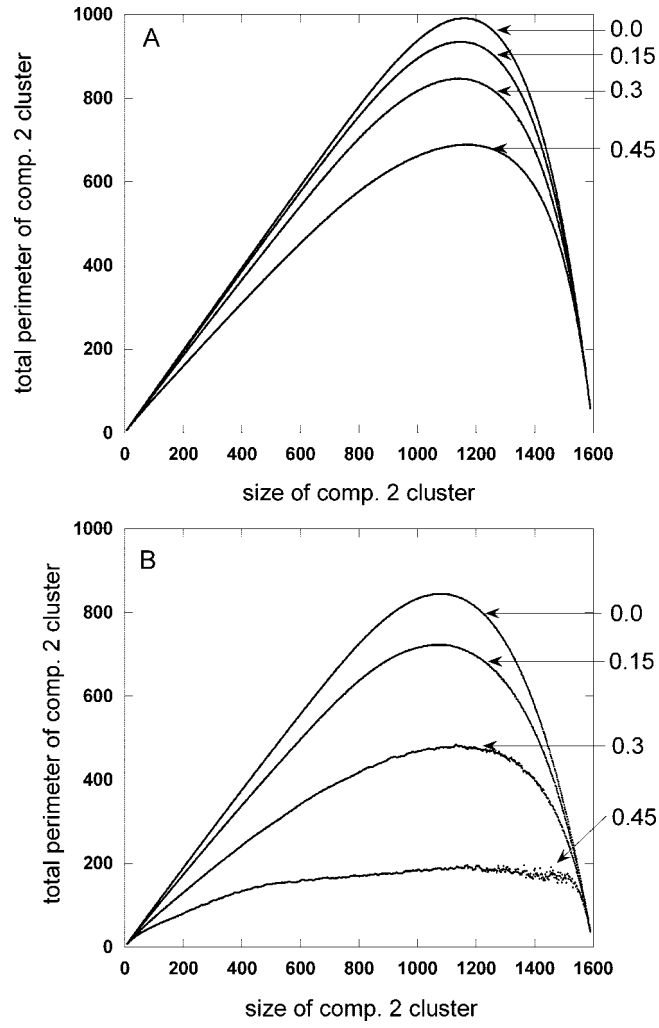

Figure 2. Average total perimeter of the largest component 2 cluster plotted against the cluster size. Each curve is labeled by the respective value of the cooperativity parameter, w/kT $\{=[E_{12} - (E_{11} + E_{22})/2]/kT\}$, where E_{ij} is the interaction between nearest neighbor chains of component i and j. (a and b) Monomer and dimer models of the two-component lipid bilayer, respectively.

The curves of the monomer model taken at $0 < w/kT < 1.1$ are qualitatively similar, but the above-described sudden changes in the outer and inner perimeters are less sharp.

At $w/kT \geq 1.1$, the outer perimeter curves are flat from cluster size 600 to 1000. In this size range the clusters are topologically band-like (Figure 5h) and the outer perimeter of the cluster is constant, about 100. At $w/kT \geq 1.1$, the clusters are compact; i.e., the inner perimeter is rather small. For example, at $w/kT = 1.4$, the inner perimeter slightly increases from 0 to 3 while the cluster size increases from 0 to 1500.

In the case of the dimer model the band-like cluster appears at $w/kT \geq 0.36$ (see Figure 3b and 4b). The outer perimeter tends to remain constant, while the inner perimeter slowly increases. For example, at $w/kT = 0.45$ the outer perimeter is constant, $\approx 135 \pm 5$, from cluster size 470 to 1130, i.e. in this size range the cluster has a band shape. Within the same cluster size range the inner perimeter slowly increases from 20 to 50, i.e. it proportionally increases with the width of the band-like cluster. The value of the outer perimeter shows that there is only one band (no parallel bands). About 67 lattice points form

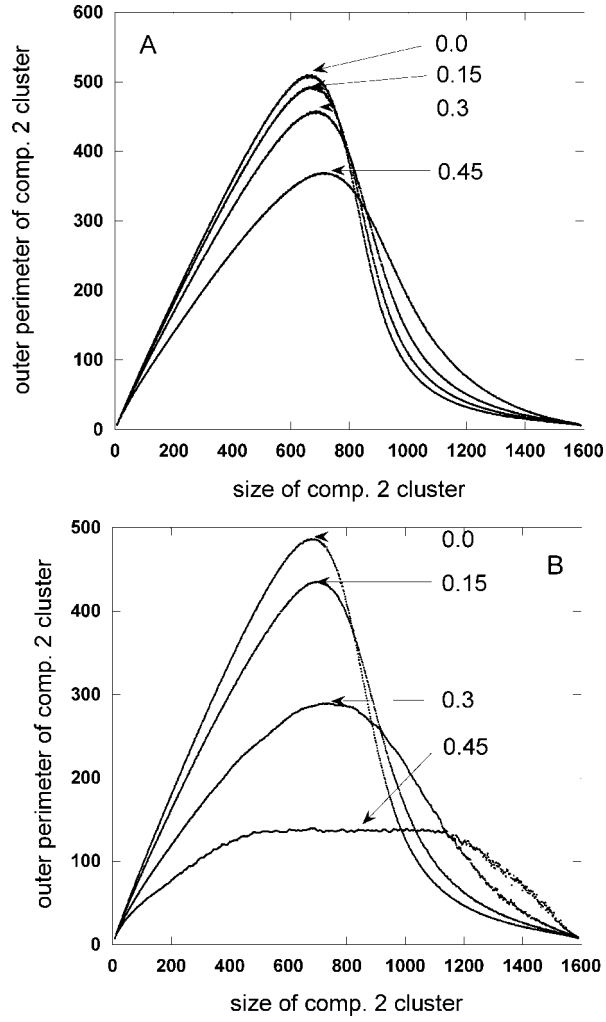

Figure 3. Average outer perimeter of the largest component 2 cluster plotted against the cluster size. Each curve is labeled by the respective value of *w/kT* parameter. (a and b) Monomer and dimer models of the two-component lipid bilayer, respectively.

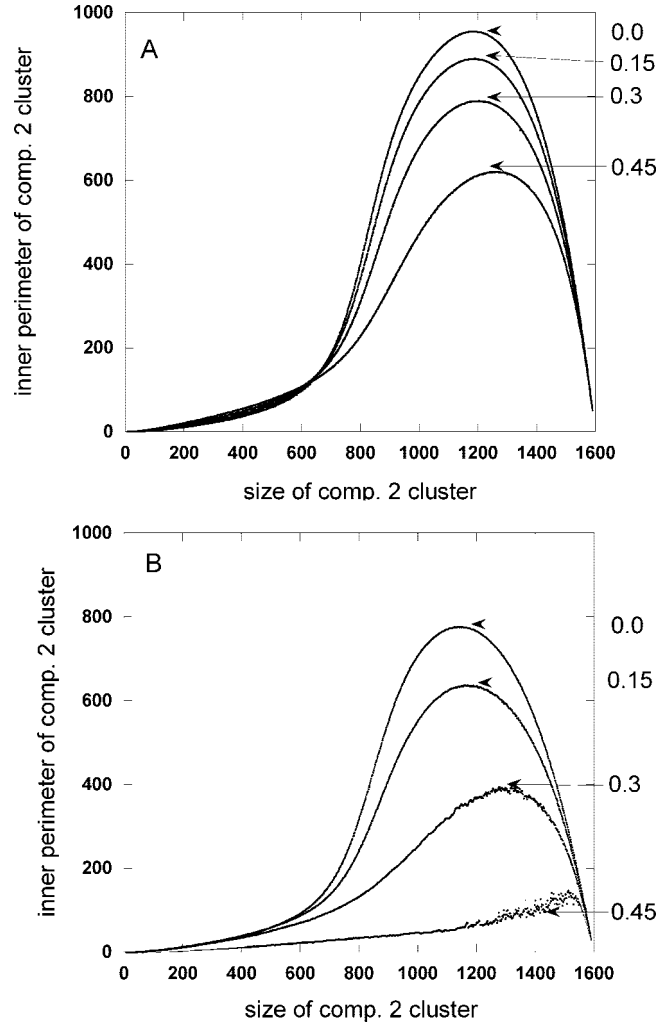

Figure 4. Average inner perimeter of the largest component 2 cluster plotted against the cluster size. The inner perimeter is equal with the total perimeter minus the outer perimeter. Each curve is labeled by the respective value of *w/kT* parameter. (a and b) Monomer and dimer models of the two-component lipid bilayer, respectively.

each of the two outer edges of the band. The band-edge is rugged and thus it is longer than the linear size of the lattice, $n = 40$.

Cluster Topologies and Their Transitions. Parts a−e of Figure 5 show a series of snapshots from the dimer model taken at the same cooperativity parameter, $w/kT = 0$, but at different cluster sizes from 400 to 1200. In these snapshots the elements of the largest component 1 cluster are marked by yellow dots. The outer periphery of the largest component 2 cluster is marked by black dots, while dots of different colors represent the cluster elements at different depths. The inner islands of the largest component 1 and component 2 clusters are marked by white.

At *small cluster sizes* the largest component 2 cluster is a branch-like, one-dimensional object (see Figure 5a). The number of cluster points within the outer perimeter is small relative to the cluster size. To estimate the fractal dimension of the clusters in the 0−600 size range we created the double logarithmic plot of the cluster size vs the outer periphery curve (not shown). The plot results in a straight line, and its slope defines the fractal dimension of the small clusters. In Table 1 the fractal dimensions obtained for different models and cooperativity parameter values are listed. With increasing value of *w/kT*, the fractal dimension of the cluster increases from slightly higher than 1 to close to 2. This increase is much faster in the case of the dimer model. A topologically circular cluster with fractal dimension close to 2 is shown in Figure 5g.

At constant *w/kT* the dimension of the cluster can also be increased by increasing the cluster size. At *large cluster sizes* the number of cluster points within the outer perimeter is comparable to the cluster size. In this case the cluster covers almost the whole surface of the lattice with the exception of the small islands of component 1 chains (see Figure 5e). Thus with increasing cluster size the dimensionality of the cluster changes from 1 to 2. The degree of transition from 1 to 2-dimensional clusters, θ, can be characterized by the following ratio: number of cluster elements within the outer perimeter/ cluster size. At $w/kT = 0$ intermediate stages of the transition from 1 to 2 dimensions are visualized by the snapshots in Figure 5a−e. The respective θ values are indicated in the figure legends.

It was noticed in the previous section that above cluster size 700 the outer perimeter of the cluster sharply decreases while the inner perimeter sharply increases. The degree of this transition from outer to inner perimeter can be characterized by θ_p, the internal to total perimeter ratio. On the (*w/kT, cluster size/lattice size*) plane in Figure 6a,b each point of the dashed line gives the respective midpoint of this transition, i.e. where $\langle\theta_p\rangle = {}^1/_2$. To the left of the dashed line less than half of the

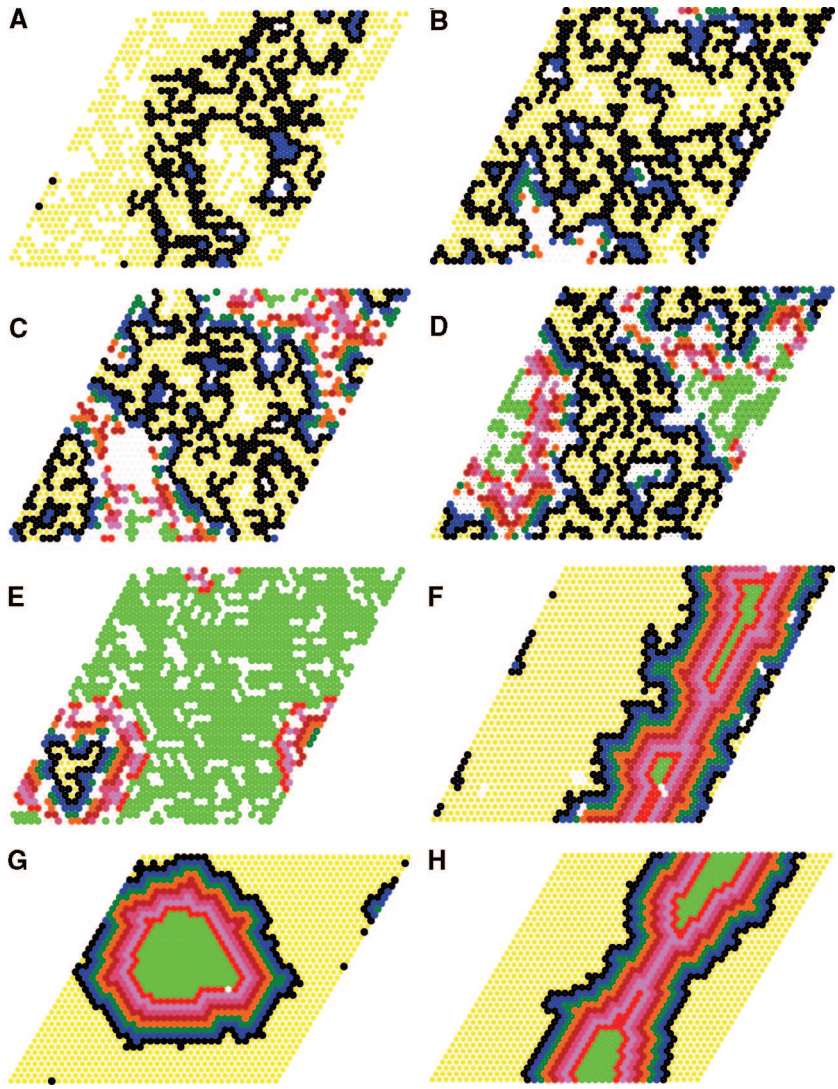

Figure 5. Snapshots of monomer and dimer model at different w/kT and cluster sizes. The size and θ and θ_p values (see definitions in the text) for the largest component 2 cluster are as follows: (a) 400, 0.07, 0.011; (b) 700, 0.18, 0.132; (c) 800, 0.48, 0.46; (d) 900, 0.58, 0.527; (e) 1200, 0.97, 0.961. Each of these snapshots was taken at $w/kT = 0$. The snapshot in part f was taken at $w/kT = 0.42$ where the size of the component 2 cluster is 800. Snapshots a−f refer to the dimer model, but the connections between the acyl chains are not shown. (g and h) Snapshots of the monomer model at cluster size 800. The snapshots in parts g and h were taken at $w/kT = 1$ and 1.2, respectively. Chains of the lipid molecules are marked by dots of the following colors: yellow (elements of the largest component 1 cluster), black (outer periphery of the largest component 2 cluster, i.e. depth 1), blue (depth 2), green (depth 3), light brown (depth 4), dark brown (depth 5), pink (depth 6), purple (depth 7), red (depth 8), and light green (depth 9 and deeper). The inner islands of the largest component 2 and component 1 clusters are marked by white.

TABLE 1: Fractal Dimensions of the Clusters in the 0−600 Size Range[a]

	monomer model		dimer model	
w/kT	Fractal dimension	Cluster size range	Fractal dimension	Cluster size range
0.0	1.0534 ± 0.001	0−600	1.0702 ± 0.001	0−600
0.15	1.0644 ± 0.001	0−600	1.1028 ± 0.001	0−600
0.3	1.0864 ± 0.001	0−600	1.2405 ± 0.002	0−600
0.45	1.1536 ± 0.0008	0−600	1.453 ± 0.0025	20−500
1.0	1.748 ± 0.0012	34−600		
1.2	1.816 ± 0.0013	34−600		
1.4	1.826 ± 0.0029	34−600		

[a] The correlation coefficient $r > 0.999$ in the case of each linear regression.

total perimeter is inner perimeter, while to the right more than half of the total perimeter is inner perimeter.

In Figure 6a,b, each point of the solid line gives the respective midpoint of the transition from 1 to 2-dimensional cluster, i.e., where $\langle\theta\rangle = {}^1/_2$. Below and to the left of this solid line the clusters are more one-dimensional, while on the other side of the solid line they are more two-dimensional.

In the region of the two-dimensional clusters in Figure 6a,b an area is separated by dash-dotted lines. In the case of the monomer and dimer model this area is situated at $w/kT \geq 1.1$ and $w/kT \geq 0.36$, respectively. The respective cluster shape in these regions is band-like. The formation of the band-like cluster is the consequence of the periodic boundary condition imposed on our model that results in a toroid geometry of the lattice. At this membrane geometry, when w/kT is high enough, two macroscopically separate clusters (the largest component 1 and largest component 2 clusters) arrange in bands to minimize the interface energy. A band-like cluster will not form in the case of planar or spherical membranes, but it can form in the case of cylindrical membranes, such as axon membranes (see also the section On the Biological Relevance of the Monomer and Dimer Models).

In general, at the same cluster size and w/kT value, the clusters of the dimer model are more compact than that of the monomer

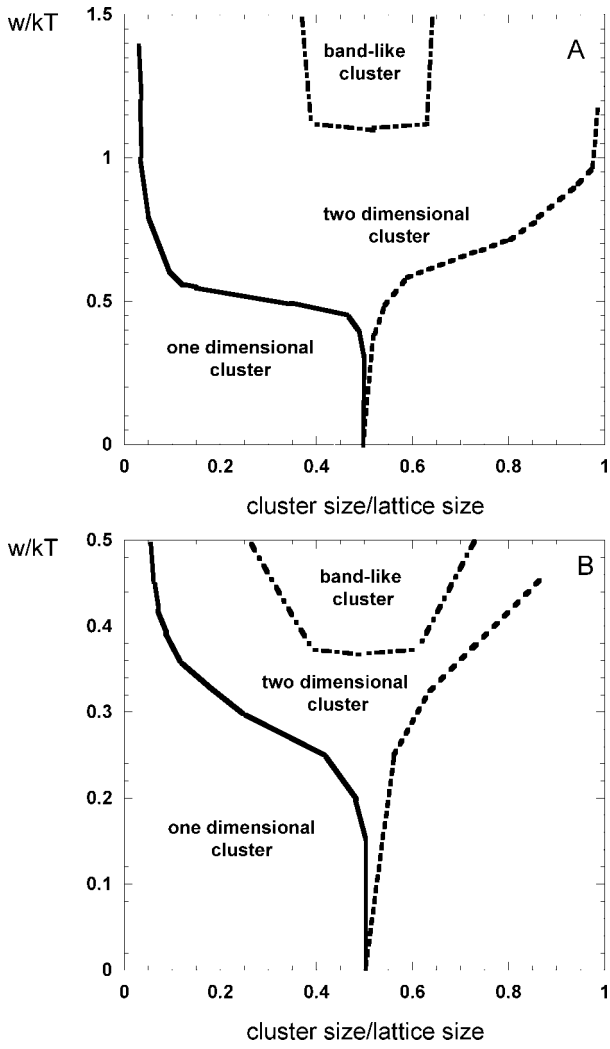

Figure 6. Diagrams of cluster topologies. On the (*w/kT*, *cluster size/lattice size*) plane each point of the solid line is defined by the midpoints of the transition from 1 to 2-dimensional cluster; i.e., $\langle\theta\rangle = 0.5$. The points of the dashed line refer to clusters where the average inner perimeter is equal to the average outer perimeter, i.e. $\langle\theta_p\rangle = 0.5$. At a given *w/kT* value, the coordinates of the left and right-hand side dash-dotted lines are defined by the beginning and end of the horizontal section of the outer perimeter curves. The region separated by the dash-dotted line refers to band-like cluster topology. (a and b) Monomer and dimer models of the two-component lipid bilayer, respectively.

model. This is because the formation of the smallest inner island requires more energy in the dimer model while the entropy gain is about the same. Note that the formation energy of the smallest inner island is *6w* and *8w* in the case of the monomer and dimer model, respectively.

Size Fluctuation of the Largest Component 1 Cluster. At a given size of the largest component 2 cluster, the size of the largest component 1 cluster fluctuates. In Figure 7 the standard deviation from the average size of the component 1 cluster is plotted against the size of the largest component 2 cluster, where the curves belong to different *w/kT* values. Figure 7 refers to the dimer model, but the characteristics of the fluctuation curves for the monomer model are similar (not shown). Each fluctuation curve in Figure 7 has two maxima, belonging to the two major mechanisms that alter the size of the largest component 1 cluster. The maximum at the smaller cluster sizes is the result of cluster branch opening/closing. At these sizes the cluster shape is branch-like (see Figure 5a). When a branch of the largest component 2 cluster closes, forming a loop, it entraps part of

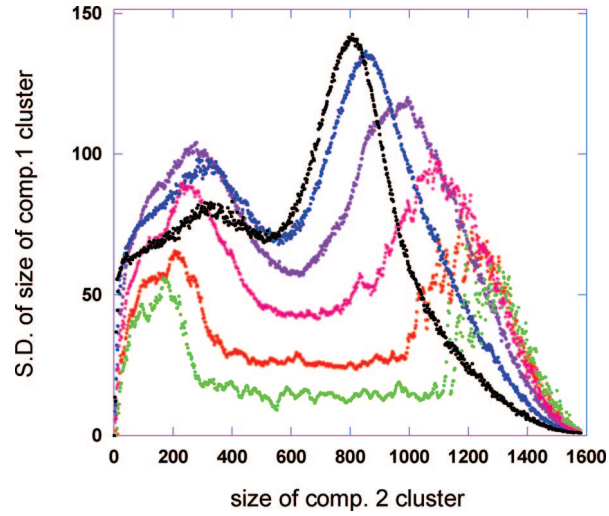

Figure 7. Cluster size fluctuation of the largest component1 cluster. In the case of the dimer model the standard deviation from the average size of the largest component 1 cluster is plotted against the size of component 2 cluster. Standard deviations calculated at different *w/kT* values are color coded as follows: black ($w/kT = 0$), blue ($w/kT = 0.15$), purple ($w/kT = 0.25$), pink ($w/kT = 0.3$), red ($w/kT = 0.35$), green ($w/kT = 0.4$).

the largest component 1 cluster. This entrapped part becomes an inner island of the largest component 2 cluster.

The other maximum of the fluctuation curves at larger cluster sizes is the consequence of separation/coalescence of the inner islands of the largest component 2 cluster. When two inner islands coalesce the formed cluster may become larger than the originally largest component 1 cluster; i.e., it becomes the largest component 1 cluster. As a consequence the original outer periphery of the largest component 2 cluster becomes part of the inner periphery. Also, the depths of the cluster elements will be reclassified; i.e., depths of the cluster elements of the original periphery become deeper than 1. The mechanism described here is identical with the internalization of the outer periphery of the largest component 2 cluster and thus the location of the fluctuation maximum at any *w/kT* coincides with the midpoint of the transition from outer to inner periphery represented by the dashed line in Figure 6b.

Depth Analysis of the Cluster. The inner structure of the cluster can be characterized by using the concept of cluster point depth. By means of this concept (i) one can classify every cluster point according to its distance from the outer periphery, (ii) define the central point(s) of a cluster of any shape, and (iii) calculate the cluster's minimal linear size (MLS).

Let us consider those snapshots of the Monte Carlo simulation where the size of the largest component 2 cluster is the same, *N*. One can determine d_k, the number of cluster points at depth *k*, for each of these clusters and calculate the average number of cluster points that belong to the same depth, $\langle d_k\rangle$. In Figure 8, $\langle d_k\rangle$ is plotted against the depth, *k*. Each curve in Figure 8 belongs to different cluster sizes, *N*.

Depending on the cluster topology there are 4 types of $\langle d_k\rangle$ curves. In the case of one-dimensional clusters $\langle d_1\rangle \approx N$ and $\langle d_k\rangle$ quickly decreases to zero. The average MLS of these clusters is small. In the case of topologically circular clusters $\langle d_k\rangle$ decreases less quickly to zero (see Figure 8e), and thus the average MLS is larger.

In the case of a band-like cluster $\langle d_k\rangle$ quickly decreases and levels off at $\langle d_k\rangle \geq 2n$, where *n* is the linear size of the lattice

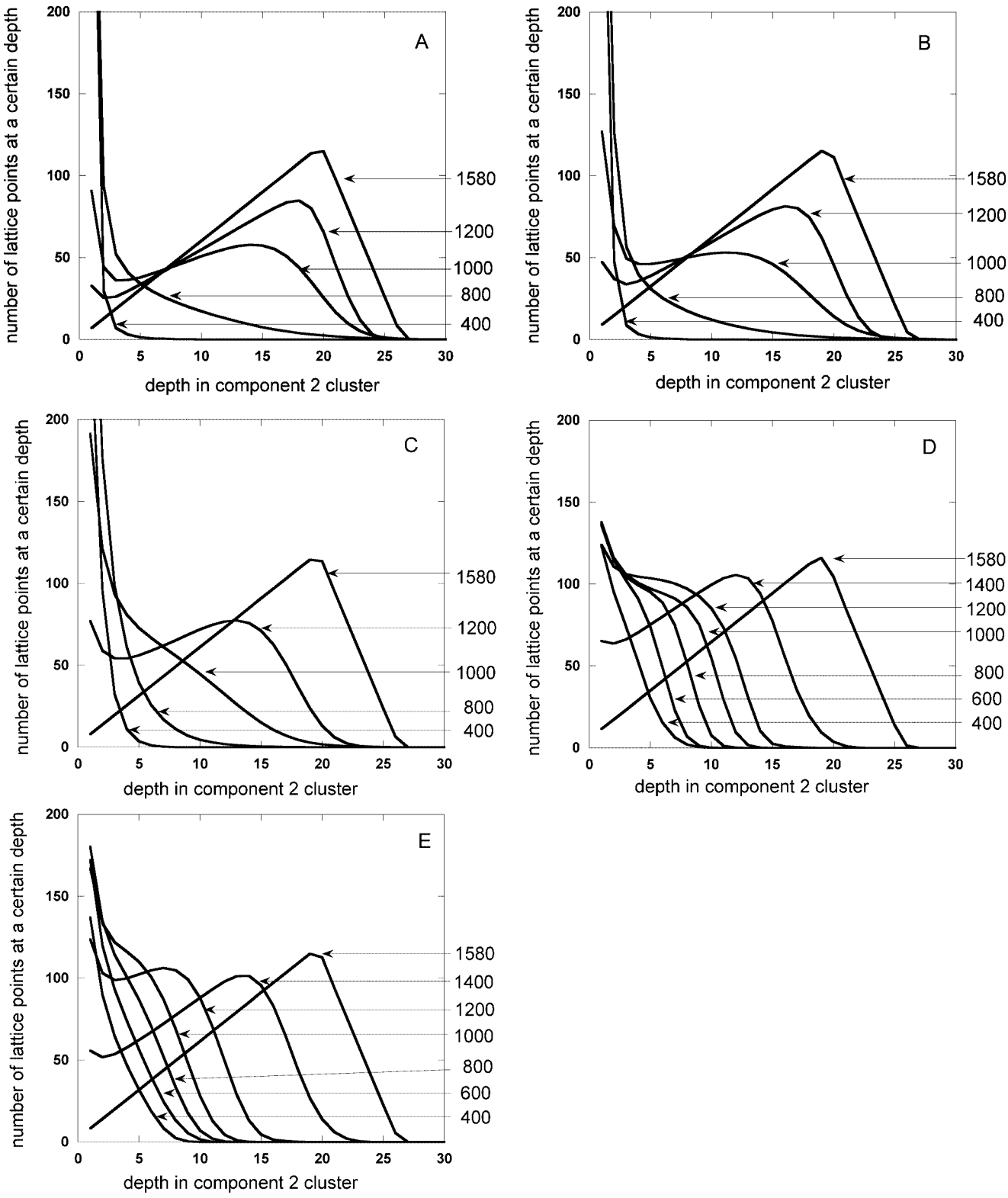

Figure 8. Average number of cluster points that belong to the same depth, $\langle d_k \rangle$, is plotted against the depth, k. Each curve belongs to a certain cluster size. The curves are labeled by the respective cluster sizes. (a and b) Monomer and dimer models of the two-component lipid bilayer, respectively, at $w/kT = 0$. (c and d) Monomer and dimer models of the two-component lipid bilayer, respectively, at $w/kT = 0.45$. (e) Monomer model of the two-component lipid bilayer at $w/kT = 0.6$.

(Figure 8d). Then $\langle d_k \rangle$ quickly decreases to zero at a cutoff depth, k_{cut}. The average MLS and average width of the band-like cluster is slightly larger than $2k_{cut}$, and it linearly increases with cluster size, N.

In the case of a large planar cluster that contains a few small inner islands (e.g., at Figure 5e), after a short decrease $\langle d_k \rangle$ linearly increases to a maximum at $k \approx n/2$. The slope of the linearly increasing section is ≈6. On a triangular lattice when the outer perimeter is small relative to the cluster size and inner islands are very small and rare $\langle d_{k+1} \rangle - \langle d_k \rangle \approx 6$. Thus the maximum of the curve is $\langle d_{n/2} \rangle \approx 6(n/2)$, i.e., about 120 in our case. After reaching the maximum, $\langle d_k \rangle$ decreases linearly, with

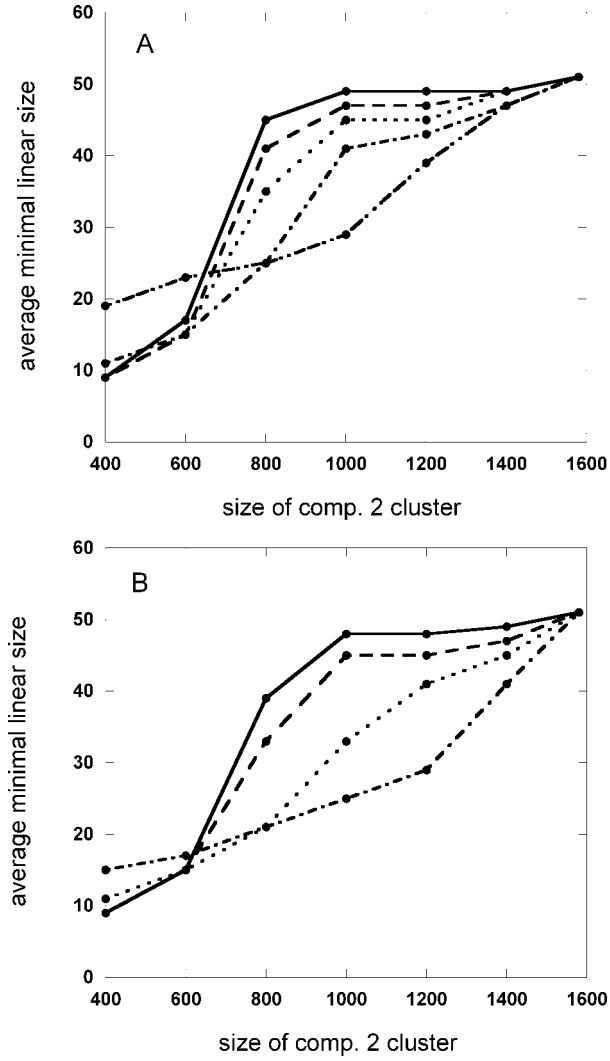

Figure 9. Average minimal linear size (MLS) of the cluster plotted against the size of the largest component 2 cluster. $w/kT = 0.0$ (solid line), $w/kT = 0.15$ (dashed line), $w/kT = 0.3$ (dotted line), $w/kT = 0.45$ (dash-dotted line), and $w/kT = 0.6$ (double dash-dotted line). (a and b) Monomer and dimer models of the two-component lipid bilayer, respectively.

a slope of -18, to 0. The average MLS of these clusters is slightly less than $4n/3$.

In Figure 9, the average MLS of the cluster is plotted against the cluster size. At small cluster sizes it slowly, linearly increases with cluster size. However, at larger cluster sizes, it starts increasing with a higher rate as the internalization of the outer periphery takes place. As we mentioned above the average MLS of the band-like cluster is about $2k_{cut}$ and it is directly proportional to the cluster size.

Local Density in the Cluster. Let us consider those snapshots of the Monte Carlo simulation where the size of the largest component 2 cluster is the same, N. By means of eq 8, one can determine $\langle\rho^k\rangle$ the average local density of component 1 at depth k, for each of these clusters and calculate the average of the $\langle\rho^k\rangle$'s, i.e. the double average, of the local density, $\langle\langle\rho^k\rangle\rangle$. In Figure 10, $\langle\langle\rho^k\rangle\rangle$ is plotted against the depth of the cluster points, k. Each curve in Figure 10 belongs to different w/kT values. At a certain depth the local density of component 1 decreases with increasing w/kT; i.e., the cluster becomes more compact. Each curve has a local maximum at depth 1 and a global minimum at depth 2. The local maximum is present because the outer perimeter of the cluster is exclusively surrounded by component 1 molecules. The global minimum exists because the outside of depth 2 cluster points is surrounded exclusively by component 2 molecules. Note that the outer perimeter of the cluster is an unbroken chain of component 2 lattice points. The chain of depth 2 lattice points, and the chains at deeper levels, can be broken by component 1 molecules that form the inner islands of the cluster. For example in Figure 1d the chain of depth 2 cluster points (blue dots) is broken by an acyl chain of component 1 (open circle). Thus at a given w/kT $\langle\langle\rho^k\rangle\rangle > \langle\langle\rho^2\rangle\rangle$ where $k > 2$.

In the case of medium size clusters (Figure 10a,b) $\langle\langle\rho^k\rangle\rangle < \langle\langle\rho^{k+1}\rangle\rangle$ where $k > 1$; i.e., the density of component 1 increases toward the center(s) of the cluster.

The increasing density is the consequence of the frequent presence of an inner island comparable in size to the largest component 1 cluster. It was pointed out in the section Size Fluctuation of Largest Component 1 Cluster that within medium size component 2 clusters an inner island even larger than the originally largest component 1 cluster frequently forms.

In the case of very large clusters (Figure 10c,d), $\langle\langle\rho^k\rangle\rangle \approx \langle\langle\rho^{k+1}\rangle\rangle$ where $k > 4$; i.e., the inner islands are small and homogeneously distributed. The only exception is in Figure 10d at $w/kT = 0.45$ where the density of component 1 increases toward the inside of the largest component 2 cluster of size 1400. Again the reason is that at this cluster size and w/kT value an inner island even larger than the originally largest component 1 cluster frequently forms within the largest component 2 cluster (see Figure 7).

In the case of topologically circular and band-like clusters w/kT is large and $\langle\langle\rho^k\rangle\rangle \approx 0$ at $k > 1$; i.e., the density of the inner islands is close to zero.

Percolation Frequency of the Cluster. The percolation properties of the clusters affect the equilibrium poise and rates of in-plane reactions and interactions, which may be physiologically important in biological membranes.[5,35]

In Figure 11 the percolation frequency, is plotted against the cluster size. In Figure 11 each curve belongs to different values of the w/kT parameter. The percolation frequency curves, obtained for the monomer model, have similar characteristics (see Figure 11a) within the range of $0 < w/kT \leq 0.45$. The sigmoid shape curves are slightly shifted toward larger cluster sizes because the clusters become more compact with increasing w/kT values. At $w/kT = 0.6$, the percolation frequency curve sharply increases. The onset of percolation shifts toward a significantly higher cluster size, while the location of percolation completion does not change.

The percolation frequency curves of the dimer model are similar at $w/kT < 0.36$. However, from $w/kT = 0.36$, the slope of the sigmoid curve increases with increasing w/kT, i.e. less number of component 2 molecules are able to form a band-like cluster. Also in this parameter range the fluctuation of the percolation frequency increases. In Figure 11b the dashed lines are smoothed curves fitted to the results of the simulations. It is important to note that, in the case of $w/kT = 0.45$, 50% of the snapshots become percolated at cluster size ≈ 470. Also at this cluster size the cluster shape becomes band-like (see Figure 3b). Thus band-like clusters are percolated clusters. At $w/kT > 0.36$, the percolation frequency curves sharply change and band-like cluster appear as a result of a very small change in the membrane composition.

In the case of both models, with increasing w/kT, the percolation curves get sharper. However, in the case of the monomer model the onset of the percolation appears at a higher cluster size, while in the case of the dimer model the completion of the percolation takes place at a lower cluster size.

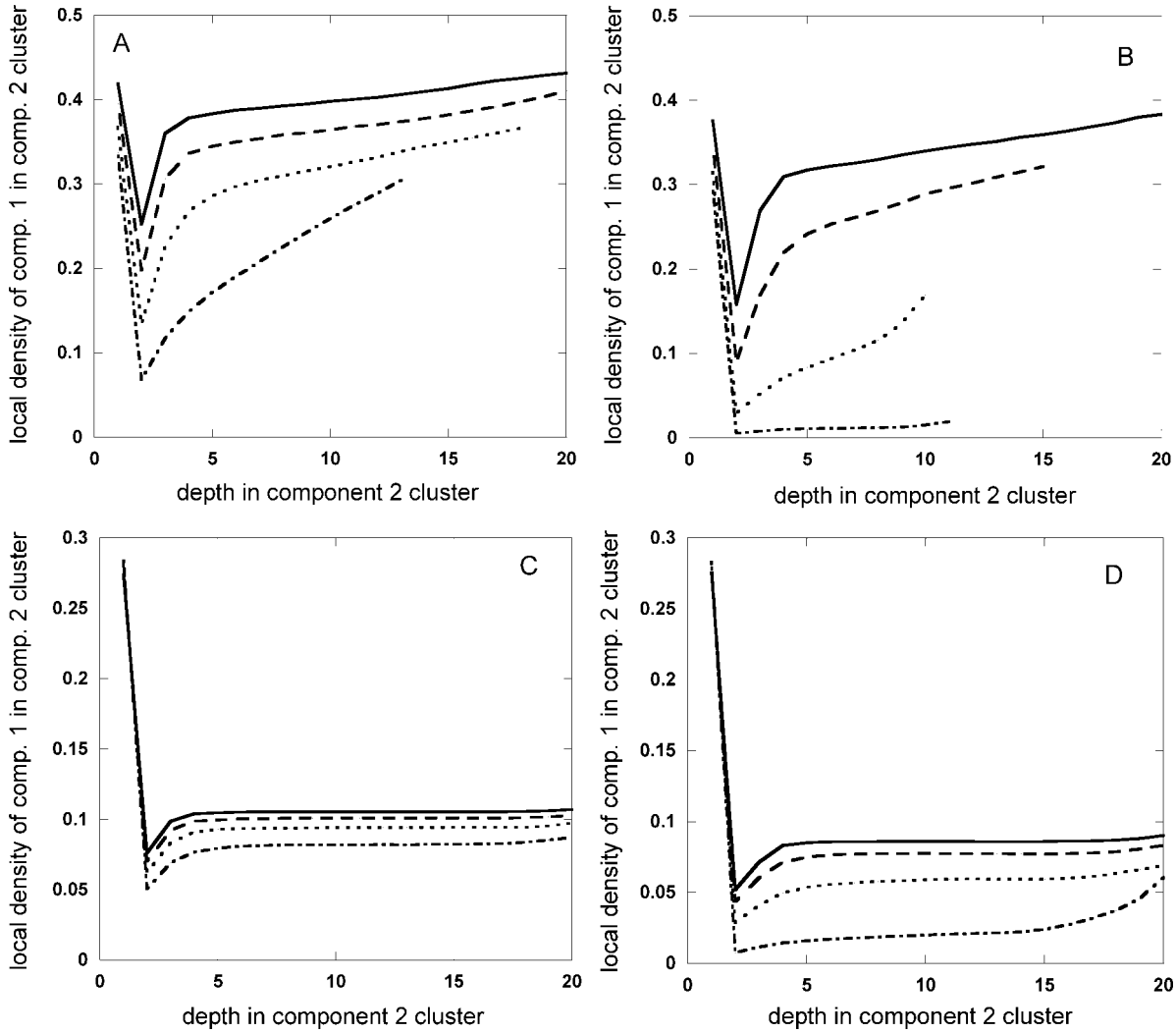

Figure 10. Average local density of component 1 at a certain depth, $\langle\langle\rho^k\rangle\rangle$, plotted against the depth, k, of the cluster points in the largest component 2 cluster. $w/kT = 0$ (solid line), $w/kT = 0.15$ (dashed line), $w/kT = 0.3$ (dotted line), and $w/kT = 0.45$ (dash-dotted line). (a and b) Monomer and dimer models of the two-component lipid bilayer, respectively, at cluster size 800. (c and d) Monomer and dimer models of the two-component lipid bilayer, respectively, at cluster size 1400.

On the Biological Relevance of the Monomer and Dimer Models. The lipid part of biological membranes is composed primarily from lipid molecules each containing two acyl chains. For example in a human erythrocyte the outer layer of the lipid matrix is largely composed of phosphatidyl−choline and sphingomyelin whereas the cytoplasmic layer contains phosphatidyl−ethanolamine, phosphatidyl−serine, and phosphatidyl−inositol;[36] i.e., each major component is a double-chain lipid. It is generally believed that biological membranes are mainly formed by double-chain lipids because the overall shape of these molecules is close to cylindrical and thus their aggregation results in cell-like large unilamellar vesicles, i.e. bilayers with a small curvature.[15] At physiological conditions the membrane is primarily in the fluid phase and thus the cross sectional area of the lipid molecules is similar. The lipid molecules are closely packed in the membrane in order to minimize the contact between the hydrophobic membrane interior and the hydrophilic extra- and intracellular space. When double-chain lipid molecules of similar cross-section are closely packed the position of the acyl chains define a triangular lattice.[16]

Both the monomer and dimer models are coarse grained lattice models of a layer of lipid bilayers. Using properly chosen model parameters both models can simulate the thermodynamic properties, such as phase diagrams, of the bilayers in quantitative agreement with experimental data.[18,19,23,24] Different parameter sets are needed because the mixing entropy of the components is different in the two models. From a microscopic point of view dimers give a better representation of phospholipid molecules than monomers and thus the mixing entropy calculated from the dimer model should be closer to the real value. The diagrams in Figure 6 show that similar sets of cluster topologies can be realized by both models. However, there are quantitative differences: (i) the clusters of the dimer model are more compact respective clusters of the monomer model; (ii) the band-like clusters appear at a much higher w/kT value in the case of the monomer model. As we mentioned above band-like clusters appear because of the toroid geometry of the lattice. The geometry of spherical and planar membranes does not support the formation of band-like clusters but membranes of a cylindrical shape do. Thus at high enough w/kT values, one can expect the formation of band-like clusters; for example in the case of axon membranes. Since band-like clusters appear/disappear as a result of a very small change in the membrane composition, one may speculate that this sudden switching has biological importance. For example, the formation of a band-like cluster in the axon membrane can block the longitudinal diffusion of components that are different from the band forming lipid.

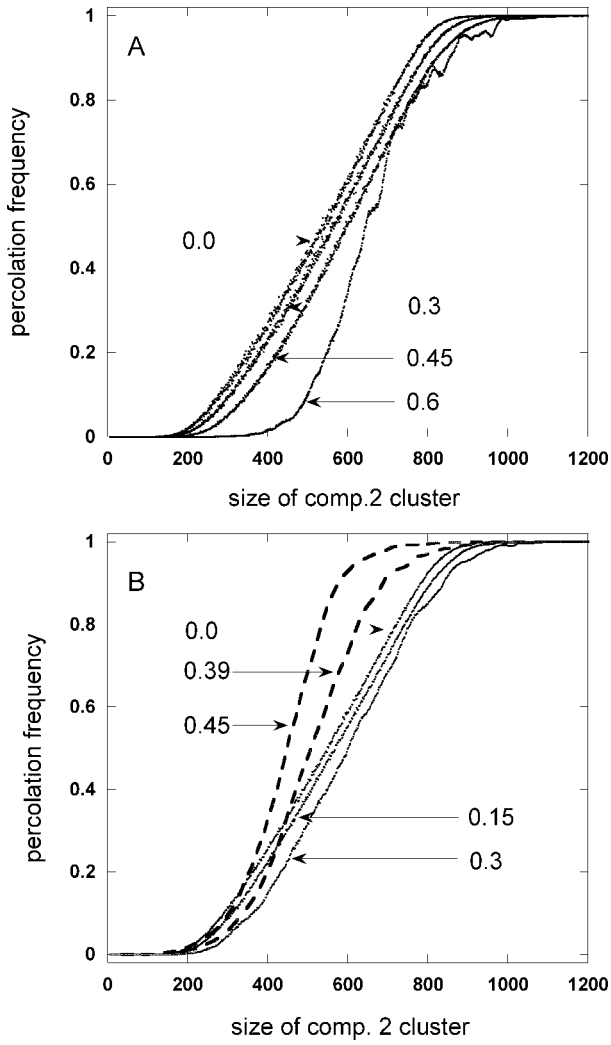

Figure 11. Percolation frequency of the largest component 2 cluster plotted against the cluster size. Each curve is labeled by the respective values of the *w*/*kT* parameter. (a and b) Monomer and dimer models of the two-component lipid bilayer, respectively. The dashed lines are smoothed curves fitted to the results of the simulations.

In 1999, we developed a dimer model of DMPC/DSPC mixtures[23] that calculated the excess heat capacity curves in agreement with experimental results. In the model at $T = 300$ K the following values of the *w*/*kT* parameter were utilized: 0.23 (in the pure gel phase region), 0.13 (in the pure fluid phase region), and 0.55 (in the gel-fluid mixed phase region).

On the basis of these parameter values and the diagram in Figure 6b, one can expect that while clusters are in the pure gel or pure fluid phase the band-like cluster topology cannot form. It can form in the gel-fluid mixed phase region. It is important to note, however, that the assumption of the triangular lattice is questionable in the mixed phase region because the cross section of the gel state molecules is considerably smaller than that of the fluid state molecules.[37] We also note that the above *w*/*kT* values refer to a two-component bilayer where the acyl chains of the components are saturated. One can expect larger *w*/*kT* values when the acyl chains of the components are more different, such as component 1 has saturated acyl chains and component 2 has unsaturated acyl chains. In systems like this, *w*/*kT* can be large enough to get a band-like cluster in the pure gel or pure fluid phase.

Conclusions

Clusters of two-component phospholipid bilayers were simulated by two Ising-type lattice models: the monomer and the dimer model. Monte Carlo techniques were applied to calculate thermodynamic averages of global and local characteristics of the largest component 2 cluster (such as outer/inner perimeter, percolation, minimal linear size, local density) and compare the results obtained by the two models. A new method was developed to characterize the inner structure of the clusters. Each point of a cluster was classified based on its shortest distance (or depth) from the cluster's outer perimeter. Then local cluster properties, such as density, were calculated as a function of the depth. The depth analysis revealed that toward the cluster interior the average density usually decreases in midsize clusters and remains constant in very large clusters. On the basis of the simulations the following typical cluster topologies were identified at different cluster sizes and cooperativity parameter values: (i) branch-like, (ii) circular, (iii) band-like, and (iv) planar.

We did not find qualitative differences between the cluster structures in the dimer and monomer model. However, at the same cluster size and cooperativity parameter value the cluster of the dimer model is more compact. The cluster properties of the dimer model are different from that of the monomer model because of the lower mixing entropy and higher formation energy of an elementary inner island.

Acknowledgment. I thank Profs. Stuart Sealfon and Fernand Hayot for critical evaluation of the manuscript before its submission. I acknowledge the use of the Mount Sinai School of Medicine Computational Biology Shared Resource Facility to conduct the Monte Carlo simulations described in this work. I am very grateful for the unceasing support from Sri Chinmoy and Suchitra Sugár, MSc. This work was supported by NIH grants to Profs. Howard Brockman (HL49180) and Rhoderick Brown (NIH/NIGMS GM45928 and NIH/NCI CA121493), and by an NIH contract (NIH/NIAID HHSN266200500021C—Principal Investigator: Prof. Stuart Sealfon).

References and Notes

(1) Chapman, D. Liquid crystalline properties of phospholipids and biological membranes. *Symp. Faraday. Soc.* **1971**, *5*, 163–174.

(2) Trauble, H. Phasenumwandlungen in Lipiden. Mogliche Schaltprozesse in Biologischen Membranen. *Naturwissenschaften* **1971**, *58*, 277–284.

(3) Melo, E. C.; Lourtie, I. M.; Sankaram, M. B.; Thompson, T. E. Effects of domain connection and disconnection on the yields of in-plane biomolecular reactions in membranes. *Biophys. J.* **1992**, *63*, 1506–1512.

(4) Vaz, W. L.; Almeida, P. F. F. Phase topology and percolation in multi-phase lipid bilayers: Is the biological membrane a domain mosaic. *Curr. Opin. Struct. Biol.* **1993**, *3*, 482–488.

(5) Thompson, T. E.; Sankaram, M.; Biltonen, R.; Marsh, D.; Vaz, W. Effects of domain structure on in-plane reactions and interactions. *Mol. Membr. Biol.* **1995**, *12*, 157–162.

(6) Hinderliter, A.; Biltonen, R. L.; Almeida, P. F. Lipid modulation of protein-induced membrane domains as a mechanism of signal transduction. *Biochemistry* **2004**, *43*, 7102–7110.

(7) Salinas, D. G.; Feunte, M. D. L.; Reyes, J. G. Changes of enzyme activity in lipid signaling pathways related to substrate reordering. *Biophys. J.* **2005**, *89*, 885–894.

(8) Kamp, J.A.F.O.D.; Kauerz, M. T.; Deenen, L. V. Action of pancreatic phospholipase A2 on phosphatidylcholine bilayers in different physical states. *Biochim. Biophys. Acta* **1975**, *406*, 169–177.

(9) Lichtenberg, D.; Romero, G.; Menashe, M.; Biltonen, R. L. Hydrolysis of dipalmitoylphosphatidylcholine large unilamellar vesicles by porcine pancreatic phospholipase A2. *J. Biol. Chem.* **1986**, *261*, 5334–5340.

(10) Grainger, D.; Reichert, A.; Ringsdorf, H.; Salesse, C. An enzyme caught in action: Direct imaging of hydrolytic function and domain formation of phospholypase A2 in phosphatidylcholine monolayers. *FEBS Lett.* **1989**, *252*, 73–82.

(11) Cannon, B.; Hermansson, M.; Gyorke, S.; Somerharju, P.; Virtanen, J. A.; Cheng, K. H. Regulation of calcium channel activity by lipid domain formation in planar lipid bilayers. *Biophys. J.* **2003**, *85*, 933–942.

(12) Bolen, E. J.; Sando, J. J. Effect of phospholipids unsaturation on protein kinase C activation. *Biochemistry* **1992**, *31*, 5945–5951.

(13) Dibble, A. R. G.; Hinderliter, A. K.; Sando, J.; Biltonen, R. L. Lipid lateral heterogeneity in phosphatidylcholine/phosphatidylserine/diacylglycerol vesicles and its influence on protein kinase C activation. *Biophys. J.* **1996**, *71*, 1877–1890.

(14) Tang, D.; Dean, W. L.; Borchman, D.; Paterson, C. A. The influence of membrane lipid structure on plasma membrane $Ca^{2+}-$ATPase activity. *Cell Calc.* **2006**, *39*, 209–216.

(15) Israelachvili, J. N. In *Intermolecular and Surface Forces*; Academic Press: 1985. Chapter 16.

(16) Ruocco, M. J.; Shipley, G. G. Characterization of the subtransition of hydrated dipalmitoylphosphatidylcholine bilayers. *Biophys. J.* **1982**, *691*, 309–320.

(17) Ising, E. Beitrag zur Theorie des Ferromagnetismus. *Z. Phys.* **1925**, *31*, 253–258.

(18) Pink, D. A.; Green, T. J.; Chapman, D. Raman scattering in bilayers of saturated phosphatidylcholines. Experiment and Theory. *Biochemistry* **1980**, *19*, 349–357.

(19) Jorgensen, K.; Sperotto, M. M.; Mouritsen, O. G.; Ipsen, J. H.; Zuckermann, M. J. Phase equilibria and local structure in binary lipid bilayers. *Biochim. Biophys. Acta* **1993**, *1152*, 135–145.

(20) Risbo, J.; Sperotto, M.; Mouritsen, O. G. Theory of phase equilibria and critical mixing points in binary lipid membranes. *J. Chem. Phys.* **1995**, *103*, 3643–3656.

(21) Jorgensen, K.; Mouritsen, O. G. Phase separation dynamics and lateral organization of two-component lipid membranes. *Biophys. J.* **1995**, *95*, 942–954.

(22) Jerala, R.; Almeida, P. F. F.; Biltonen, R. L. Simulation of the gel-fluid transition in a membrane composed of lipids with two connected acyl chains: application of a dimmer-move step. *Biophys. J.* **1996**, *71*, 609–615.

(23) Sugar, I. P.; Thompson, T. E.; Biltonen, R. L. Monte Carlo simulation of two-component bilayers: DMPC/DSPC mixtures. *Biophys. J.* **1999**, *76*, 2099–2110.

(24) Sugar, I. P.; Biltonen, R. L. Structure-function relationships in two-component phospholipids bilayers. A Monte Carlo simulation approach using a two-state model. *Methods Enzymol.* **2000**, *323*, 340–372.

(25) Sugar, I. P.; Michonova-Alexova, E.; Chong, P.L.-G. Geometrical properties of gel and fluid clusters in DMPC/DSPC bilayers: Monte Carlo simulation approach using a two-state model. *Biophys. J.* **2001**, *81*, 2425–2441.

(26) Sugar, I. P.; Biltonen, R. L. Lateral diffusion of molecules in two-component lipid bilayer: A Monte Carlo simulation study. *J. Phys. Chem. B* **2005**, *109*, 7373–7386.

(27) Michonova-Alexova, E. I.; Sugar, I. P. Component and state separation in DMPC/DSPC lipid bilayers: A Monte Carlo simulation study. *Biophys. J.* **2002**, *83*, 1820–1833.

(28) Seeger, H. M.; Fidorra, M.; Heimburg, T. Domain size and fluctuations at domain interfaces in lipid mixtures. *Macro. Symp.* **2005**, *219*, 85–96.

(29) Hac, A. E.; Seeger, H. M.; Fidorra, M.; Heimburg, T. Diffusion in two-component lipid membranes - A fluorescence correlation spectroscopy study and Monte Carlo simulation study. *Biophys. J.* **2005**, *88*, 317–333.

(30) Freire, E.; Snyder, B. Estimation of the lateral distribution of molecules in two-component lipid bilayers. *Biochemistry* **1980**, *19*, 88–94.

(31) Jan, N.; Lookman, T.; Pink, D. A. On computer simulation methods used to study models of two-component lipid bilayers. *Biochemistry* **1984**, *23*, 3227–3231.

(32) Sugar, I. P.; Biltonen, R. L.; Mitchard, N. Monte Carlo simulations of membranes: phase transition of small unilamellar dipalmitoylphosphatidylcholine vesicles. *Methods Enzymol.* **1994**, *240*, 569–593.

(33) Metropolis, M.; Rosenbluth, A. W.; Rosenbluth, M. N.; Teller, A. N.; Teller, E. *J. Chem. Phys.* **1953**, *21*, 1087–1092.

(34) Binder, K.; Stauffer, D. Monte Carlo studies of "random" systems. In *Applications of the Monte Carlo Method in Statistical Physics*; Binder, K., Ed.; Springer-Verlag: Berlin, Heidelberg, Germany, New York, and Tokyo, 1987; Chapter 8.

(35) Schram, V.; Lin, H.-N.; Thompson, T. E. Topology of gel phase domains and lipid mixing properties in phase-separated two-component phosphatidylcholine bilayers. *Biophys. J.* **1996**, *71*, 1811–1822.

(36) Bretscher, M. Asymmetrical lipid bilayer structure for biological membranes. *Nat. New Biol.* **1972**, *263*, 11–12.

(37) Nagle, J. F.; Tristram-Nagle, S. Structure of lipid bilayers. *Biochim. Biophys. Acta* **2000**, *1469*, 159–195.

JP800945J